CoSMIR Performance During the GPM OLYMPEX Campaign

Rachael A. Kroodsma, Matthew A. Fritts, Jared F. Lucey, Mathew R. Schwaller, Troy J. Ames, Caitlyn M. Cooke, *Student Member, IEEE*, and Lawrence M. Hilliard

***Abstract*—The airborne Conical Scanning Millimeter-wave Imaging Radiometer (CoSMIR) has participated in the Global Precipitation Measurement (GPM) Olympic Mountains Experiment (OLYMPEX) from November to December, 2015, with great success. With similar channels as that of the GPM Microwave Imager (GMI) at 89–183 GHz, CoSMIR served as a proxy for GMI by flying onboard the DC-8 Aircraft for a total of 17 science flights, collecting over 72 h of observations. The high-quality, calibrated brightness temperature data set is the result of several improvements made to CoSMIR prior to OLYMPEX to make the instrument more reliable. This paper describes these improvements and gives a detailed summary of the CoSMIR measurements obtained from OLYMPEX. CoSMIR experienced minor performance issues during the campaign, most of them were not excessive and only resulted in a loss of approximately 4 h of data for the entire campaign. Performance issues are discussed and shown how they were mitigated to achieve a quality data set. Comparisons of CoSMIR and GMI observations are presented to show that the CoSMIR measurements agree well with GMI. The CoSMIR data set is publicly available as a part of the OLYMPEX data suite and can reliably be used in the GPM algorithm development and related studies.**

***Index Terms*—Airborne radiometer, GPM, microwave radiometry, Olympic Mountains Experiment (OLYMPEX), precipitation.**

I. Introduction

GROUND validation (GV) is an important component of the Global Precipitation Measurement (GPM) mission, evidenced by the multiple extensive field campaigns conducted both before and after the launch of the GPM Core Observatory (CO) on February 27, 2014. The GPM mission improves upon the capabilities of its predecessor, the Tropical Rainfall Measuring Mission (TRMM), by expanding the range of observations to higher latitudes, measuring falling snow and lighter precipitation, and increasing the spatial and temporal resolution of precipitation measurements by utilizing a constellation of sensors [1], [2]. GV efforts play a critical role in improving the precipitation retrieval algorithms for GPM and validating the satellite products, ensuring that the retrieval algorithms accurately portray the conditions at the surface and throughout the atmosphere [3]. Several GV campaigns were coordinated in mid- and high-latitude regions, where TRMM did not observe, or the regions, where the precipitation retrieval algorithms have significant errors. While many GV efforts focused on installing the extensive ground networks of instruments, other campaigns utilized networks of both ground and airborne instruments. Some of these airborne instruments were sensors similar to those onboard the GPM CO, which enabled the airborne instruments to be used as proxies for the GPM CO instruments. The Conical Scanning Millimeter-wave Imaging Radiometer (CoSMIR) served as the proxy for the GPM Microwave Imager (GMI) high-frequency (89–183 GHz) channels [4] in four GPM GV campaigns from 2011 to 2015. This paper discusses the performance of CoSMIR in the last GPM GV campaign, the Olympic Mountains Experiment (OLYMPEX) [5].

CoSMIR collects observations at frequencies similar to GMI near 166 and 183 GHz that were not included in the TRMM Microwave Imager (TMI) [6], so the instrument contributes valuable information for algorithm developers using the GPM GV data. The GMI precipitation retrieval algorithm is adapted from TMI and updated to include a physical-based retrieval over land [7]. The 89–183-GHz channels are essential for overland precipitation retrieval, and CoSMIR measurements aid in understanding how these high frequencies are impacted by rain and snow from various storm structures over different terrains. Of particular interest to algorithm developers are the 166-GHz measurements. The 166-GHz channels were included in GMI to measure falling snow, as many studies showed that measurements in the 150–166-GHz range have a high sensitivity to falling snow [8], [9]. The scattering signals in the 89- and 183-GHz channels have also been shown to aid in snowfall detection over land [10]. In addition, the difference between the vertical and horizontal polarized brightness temperatures, the polarization difference (PD), is also of interest. Orientation of ice crystals in clouds produce PDs at 89 and 166 GHz, and correctly modeling this ice scattering is important for retrieval algorithms [11], [12]. In conjunction with ground-based precipitation measurements and other airborne observations, such as *in situ* cloud particle measurements and radar reflectivities, CoSMIR observations can be used to increase the understanding of how clouds and precipitation

Manuscript received July 16, 2018; revised January 20, 2019; accepted January 31, 2019. Date of publication April 17, 2019; date of current version August 27, 2019. This work was supported by the NASA Global Precipitation Measurement Mission. *(Corresponding author: Rachael A. Kroodsma.)*

R. A. Kroodsma is with the Earth System Science Interdisciplinary Center, University of Maryland at College Park, College Park, MD 20740 USA, and also with the NASA Goddard Space Flight Center, Greenbelt, MD 20771 USA (e-mail: rachael.a.kroodsma@nasa.gov).

M. A. Fritts, J. F. Lucey, M. R. Schwaller, T. J. Ames, and L. M. Hilliard are with the NASA Goddard Space Flight Center, Greenbelt, MD 20771 USA (e-mail: matthew.a.fritts@nasa.gov; jared.f.lucey@nasa.gov; mathew.r.schwaller@nasa.gov; troy.j.ames@nasa.gov; lawrence.m.hilliard@nasa.gov).

C. M. Cooke is with Northrop Grumman Aerospace Systems, Redondo Beach, CA 90278 USA (e-mail: caitlyn.cooke@ngc.com).

Color versions of one or more of the figures in this article are available online at http://ieeexplore.ieee.org.

Digital Object Identifier 10.1109/TGRS.2019.2906039

impact the radar and radiometer measurements onboard spacecraft platforms. This will aid in constraining the precipitation retrieval algorithms and improving the assumptions included in those algorithms.

In order to make a valuable contribution to the GV data set, CoSMIR needs to provide accurate and stable measurements. CoSMIR experienced some anomalies in the first three GPM GV campaigns it participated in: the Mid-latitude Continental Convective Clouds Experiment (MC3E) in 2011 [13], the GPM Cold Season Precipitation Experiment (GCPEX) in 2012 [14], and the Integrated Precipitation and Hydrology Experiment (IPHEX) in 2014 [15]. Some of the major problems encountered previously were radio frequency interference in the 183-GHz channels during MC3E, synchronization issues between the instrument computer and aircraft in IPHEX, inoperable 165-GHz horizontal polarization channel in IPHEX, and numerous data dropouts. As a result, considerable time and effort were spent prior to OLYMPEX to improve CoSMIR's performance in the campaign. The result was that CoSMIR acquired the highest quality data set from OLYMPEX compared with the prior three campaigns. The data are available at the Global Hydrology Resource Center (GHRC) (https://ghrc.nsstc.nasa.gov/home/field-campaigns) for all four campaigns.

This paper gives an extensive description of the CoSMIR instrument improvements and the measurements collected during the OLYMPEX campaign, thereby giving data users the knowledge of data availability and quality. This paper will first describe the CoSMIR instrument and improvements made prior to the OLYMPEX campaign. Next, CoSMIR's performance in OLYMPEX will be presented along with an explanation of the performance issues that we encountered. A description of how we mitigated the performance issues during the campaign and in software processing is included. Finally, the data quality will be assessed by comparing the measurements of GMI and CoSMIR.

II. Instrument

A. Description

CoSMIR is a conical and cross-track scanning total power radiometer, originally designed and built for use in the Special Sensor Microwave Imager Sounder (SSMIS) calibration and validation efforts [16]. CoSMIR was built with high-frequency channels similar to SSMIS and designed to operate on NASA's ER-2 Aircraft or another similar high-altitude aircraft. Prior to the GPM GV campaigns, the CoSMIR center frequencies were modified to be more equivalent to the GMI center frequencies and dual polarization was added for the 165.5-GHz channel [13]. Table I gives the center frequencies, bandwidth, polarization (vertical: v, horizontal: h), and noise equivalent delta temperature (NEDT) for CoSMIR. For simplicity, when referencing the CoSMIR channels in this paper, the nine channels will hereafter be identified as the following: 50, 52, 89v, 89h, 165v, 165h, 183 ± 1, 183 ± 3, and 183 ± 7 GHz.

The CoSMIR scan head contains the antennas, receivers, power conditioning, and data digitization. The scan head is mounted onto a scan pedestal, which consists of an azimuth over elevation dual-axis gimbaled scanning mechanism, two calibration targets (hot and cold), the electronics, the data acquisition, and the aircraft interface (see Fig. 1). During the OLYMPEX campaign, the scan pedestal was mounted in the DC-8 aft cargo bay. The hot calibration target was heated to approximately 320 K, and the cold calibration target was exposed to the ambient air temperature that varied from approximately 230 K to 250 K at the DC-8 cruising altitude of approximately 11.8 km. The scanning mechanism is programmable via software and can be programmed to scan strictly conical or cross track, or a combination of the two referred to as hybrid scanning. Since the GPM radiometer constellation contains both conical and cross-track sensors, the hybrid mode was chosen as the nominal mode for OLYMPEX. This gives observations over a wide variety of viewing angles to develop and validate the precipitation algorithms.

One complete rotational cycle of the instrument operating in hybrid scan mode consists of two conical scans and two cross-track scans with a hot and cold calibration target look after each earth-view scan. During this cycle, the azimuth angle rotates once through a full 360° and the elevation twice, as shown in Fig. 2. The corresponding 89v radiometer counts from a flight are also displayed in Fig. 2, along with the labels showing the conical scans (1 and 3), cross-track scans (2 and 4), hot target looks (H), and cold target looks (C). The ground track footprints for the earth-view scans are shown in

TABLE I
CoSMIR Center Frequencies (Fc), Bandwidth (BW), Polarization (Pol), and NEDT

Fc (GHz)	BW (GHz)	Pol	NEDT (K)
50.3	0.4	h	0.21
52.8	0.4	h	0.32
89.0	2.0	v/h	0.14/0.13
165.5	2.0	v/h	0.18/0.16
183.31±1	1.0	h	0.20
183.31±3	2.0	h	0.18
183.31±7	3.0	h	0.16

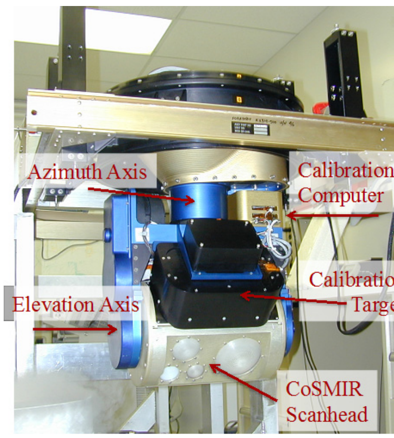

Fig. 1. Laboratory photograph of the CoSMIR scan head mounted onto the scan pedestal.

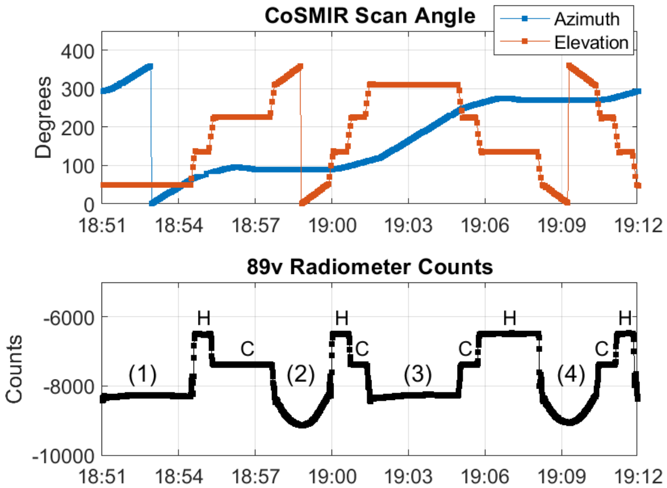

Fig. 2. CoSMIR scan pattern for one complete cycle, where the azimuth rotates once and the elevation twice. Corresponding 89v radiometer counts are shown during an OLYMPEX flight. (1) and (3): Earth-view conical scans. (2) and (4) Cross-track scans. "H" and "C" refer to the hot and cold target looks, respectively.

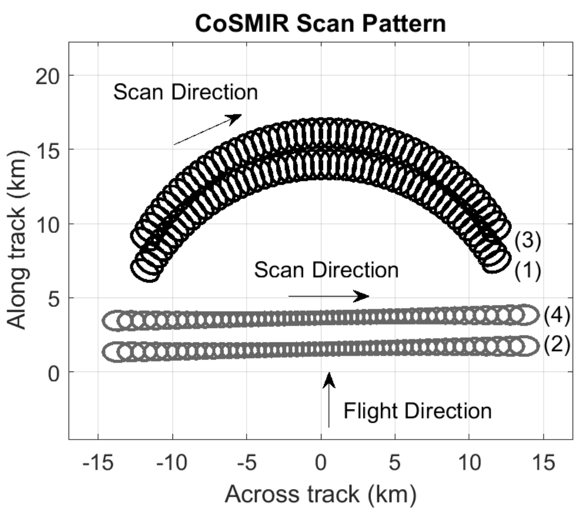

Fig. 3. CoSMIR ground track modeled for one complete rotation cycle consisting of two conical (black circles) and two cross-track (gray circles) scans. The aircraft ground speed is 200 m/s and the altitude is 11.8 km. (1)–(4): Labels in Fig. 2.

Fig. 3. At an aircraft altitude of 11.8 km, i.e., the approximate cruising altitude of the DC-8 during OLYMPEX, the footprint of the conical scan is 1.3×1.9 km, and the footprint of the cross-track scan at nadir is 0.8×0.8 km. CoSMIR greatly oversamples for both scans, and the final product is a downsampled version of the original pixels, resulting in 51 samples per scan for both conical and cross track. The conical scan swath width is 29 km and takes approximately 3 s to complete. The cross-track scan swath width is 27 km and takes approximately 2 s to complete.

For OLYMPEX, CoSMIR scanned from left to right for both conical and cross-track scans and always performed the conical scan in the forward direction at a nominal elevation angle of 49.2°. The azimuth and elevation angles shown in Fig. 2 are with respect to the instrument and not the aircraft. The instrument flips over between the first cross track and the second conical scan, so even though the azimuth angle for the second conical scan is 180° greater than the first conical scan, both conical scans are in the forward direction with respect to the aircraft. This results in the order of the calibration target looks (hot then cold versus cold then hot) being different after the first conical/cross-track scans versus the second ones, as seen in Fig. 2.

B. Recent Modifications

CoSMIR participated in the MC3E, GCPEX, and IPHEX GV campaigns with varying levels of success. While accurate observations were collected for those campaigns, data dropouts and channel malfunctions happened frequently. To improve the quality of the CoSMIR data set for OLYMPEX and to make the instrument more reliable for future field campaigns, several modifications were done to CoSMIR between the IPHEX and OLYMPEX campaigns. The CoSMIR scan head and scan pedestal were built in the early 2000s, but no major upgrades were made to the instrument since then, except to change the center frequencies to match GMI.

The major CoSMIR improvements prior to OLYMPEX included the thermal system, power system, video amplifier, and all of the 165-GHz channel hardware minus the feed. The thermal system was updated to chip heaters that allowed for better temperature control of the RF parts and saved space by eliminating the thermal control board. The power system was redesigned with a custom board to provide all required voltage regulations internal to the scan head, which improved grounding and eliminated noise in the radiometric data from the CPU clock. The video amplifiers were replaced with operational amplifiers, and the connectors were replaced with parts more suited for aircraft environment temperatures and vibrations. Finally, the 165-GHz receiver was redesigned using new technology that significantly decreased the size of the receiver by replacing the waveguide with 2.92-mm coaxial cables. These modifications significantly improved the quality of the CoSMIR data obtained from OLYMPEX compared to the prior GV campaigns.

CoSMIR was further improved after we identified and corrected two anomalies while testing the instrument in a thermal chamber prior to OLYMPEX. The first anomaly we detected was an issue with the motion control that caused the azimuth angle to travel during operation. After a few hours in the thermal chamber, we noticed that the center of the conical scan where the azimuth angle equals 0° had traveled counterclockwise by nearly 90°, meaning that CoSMIR would be scanning to the side of the aircraft rather than the front. Unfortunately, the raw data showed no evidence of this anomaly, as CoSMIR uses an incremental azimuth encoder that starts from its absolute position (0°) when the instrument is turned ON. Our solution to this problem was a software fix that pulled the absolute position two times per cycle, before each cross-track scan, so that the azimuth encoder could essentially restart. We had to slow down the scan in order to do this, adding about 1 s each time. This can be seen in Fig. 2, where there is an extended cold or hot target look prior to the cross-track scan. After detecting this motion control anomaly, we analyzed data from prior campaign flights to see if this occurred during past flights by looking at the geolocation of CoSMIR footprints over coastal crossings, where the low-frequency channels observe the surface. We noticed the azimuth angle traveling for some but not all of the flights that we have analyzed, but we could not identify why only some flights were impacted. This azimuth anomaly is a potential source of error in the geolocation for past flights, and we plan to update the past GPM field campaign data to correct this error.

The second anomaly we detected was striping in the raw counts, found when analyzing the chamber data in software. As mentioned previously, the instrument flips over every other scan to keep the conical scan in the forward direction. We noticed the raw counts jumped every other scan with a consistent offset, correlated with the instrument position. We determined that this was due to parts shifting slightly in the drum, potentially causing grounding issues. To mitigate this count offset, we electrically isolated the parts in the drum and improved the mechanical structure.

III. Aircraft Measurements

CoSMIR operated extremely well for most of the campaign. We obtained a diverse data set that includes observations from various storm structures over both land and ocean (see [5] for an in-depth discussion of the extratropical cyclone sectors observed in each flight). This section will briefly describe the flights, explain the complications that we encountered with CoSMIR, and show some of the quality control performed on the data set.

A. Description of Flights

There were a total of 17 science flights and one engineering test flight for which we collected the CoSMIR data. The engineering test flight was based out of the NASA's Armstrong Flight Research Center Palmdale, CA, USA, and is included as part of the data set. The science flights were based out of Joint Base Lewis–McChord just south of Tacoma, WA, USA. A total of 72 h and 8 min of quality-controlled CoSMIR data were collected from the flights with only about 4 h of potential science data lost due to complications with the instrument. Table II gives the date of each flight (in month/day format), the times during which CoSMIR data were collected, the GPM CO overpass time if applicable, and a summary of the instrument's performance. Nominal operation occurred when all nine channels operated for the entire flight in the hybrid scanning mode with no software or hardware issues. While this happened for less than half of the flights, most of the flights were still considered a success, as a successful flight is considered to be one where the channels necessary for science (89–183 GHz) all operated for the duration of the flight. The hardware issues and loss of 50- and 52-GHz channels did not adversely affect the collection of the necessary scientific data. A detailed explanation of the performance summary is included in Section III-B.

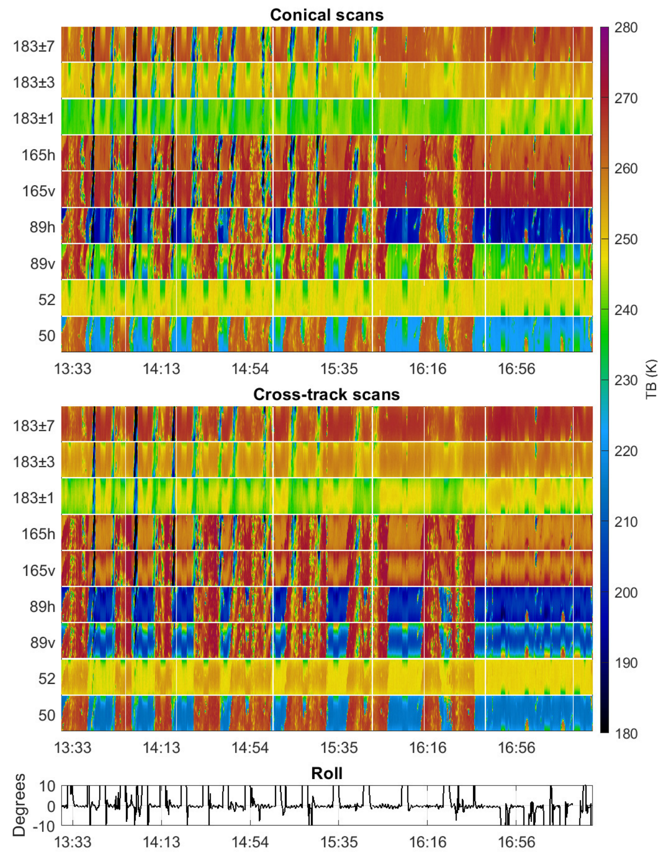

Fig. 4. CoSMIR data from a postfrontal system on December 4, 2015, for (Top) conical and (Bottom) cross-track scans. The brightness temperature for each channel is shown along with the aircraft roll.

Fig. 4 displays the CoSMIR data acquired on 12/04 during a nominal operation flight. The brightness temperatures (TBs) from the nine channels are shown for conical scans (top) and cross-track scans (bottom) along with the aircraft roll below the brightness temperature subplots. For this flight, the DC-8 flew over a postfrontal system, observing both the ocean and mountains. Several coastal crossings are apparent in the 50-, 52-, and 89-GHz channels. Early in the flight, CoSMIR observed several areas of strong convection that caused significant TB depressions in the 89-, 165-, and 183-GHz channels. These are some of the coldest TBs seen during the campaign for the 165 and 183 channels. The 12/10 flight observed slightly colder TBs during a more significant postfrontal convection event.

B. Performance Issues During OLYMPEX

The first complication we encountered during the campaign was a broken azimuth encoder. This made CoSMIR unable to scan in the azimuth direction, losing the ability to perform conical scanning. This occurred during the transit flight on 11/10, resulting in no data being collected for that flight. The following three flights on 11/12, 11/13, and 11/14 collected data in the cross-track mode only as we waited for the new azimuth encoder to arrive to fix the conical scan.

The second complication we encountered involved the DC-8 power supply for the hot target that first manifested

TABLE II
OLYMPEX DC-8 FLIGHTS WITH CoSMIR PERFORMANCE SUMMARY

Date (UTC)	CoSMIR data collected (UTC)	GPM CO overpass (UTC)	CoSMIR performance summary
11/05	20:04-22:38	--	Nominal operation Engineering test flight out of Palmdale, CA
11/12	16:09-22:17	21:16	Cross-track mode only
11/13	13:56-19:29	--	Cross-track mode only
11/14	17:13-23:17	21:06	Cross-track mode only
11/18	18:29-00:06	--	Nominal operation
11/23	15:57-21:40	--	Nominal operation
11/24	14:40-19:34	18:36	Hot target power supply issue
11/25	17:24-19:15	17:43	Hot target power supply issue Lost 52 GHz channel after 18:20 due to gain increase
12/01	20:59-01:25	--	Hot target power supply issue Lost 52 GHz channel after 22:43 Lost 50 GHz channel after 00:15
12/03	14:33-16:59	15:22	Hot target power supply issue Lost 52 GHz channel after 16:05
12/04	13:27-17:31	--	Nominal operation Fixed hot target power supply issue
12/05	14:18-15:38	15:13	Lost 52 GHz channel after 15:08 Lost 50 GHz channel after 15:31 Lost connection with archive computer at 15:38
12/08	14:08-16:33 17:44-19:24	14:11	Lost 52 GHz channel after 14:36. Lost connection with archive computer at 16:33 Rebooted successfully but hot target temperature not recorded for the rest of the flight
12/10	14:58-15:55 16:34-19:18	--	Lost connection with archive computer at 15:55. Rebooted successfully but hot target temperature not recorded for the rest of the flight
12/12	15:52-21:15	--	Nominal operation
12/13	13:54-18:15	--	Nominal operation
12/18	04:57-07:04	--	Nominal operation
12/19	01:32-03:22	2:54	Nominal operation

during the 11/24 flight. Early in the flight, the hot target temperature started dropping, an indication that the heaters for the target were not working properly. We toggled the switch on the power supply for the heaters, and this appeared to resolve the issue as the hot target temperature looked nominal for the rest of the flight. However, this became a recurring issue for several flights afterward where we would have to toggle the power supply switch early in the flight due to the hot target temperature dropping. After the 12/03 flight, we determined we had a faulty power supply for the heaters, as the output voltage was too high. We then connected the heaters to the same power supply as the archive computer. This worked properly on the 12/04 flight, but for the next three flights, the archive computer crashed mid-flight, causing a loss of recorded data, as the computer was down (more in the following). Finally, after the 12/10 flight, we obtained a new power supply for the heaters and ran the heaters and archive computer off different power supplies for the rest of the campaign (same setup as the start of the campaign). CoSMIR performed nominally for the last four flights.

The third complication involved the loss of the 50- and/or 52-GHz channels mid-flight due to the output exceeding the range of the A/D. Table II details the flights during which this happened and at what time the channel was lost. These channels have an additional amplifier compared to the other channels, so when the air temperature is very cold, the 50- and 52-GHz channels have more gain. The flights during which we lost these channels were some of the coldest air temperatures we encountered during the campaign. Even without the 50- and/or 52-GHz channels, we still consider

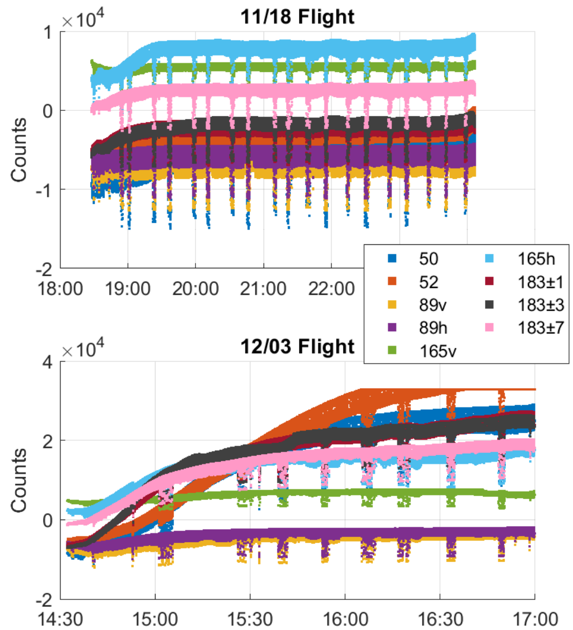

Fig. 5. Radiometer counts from (Top) nominal operation flight (11/18) and (Bottom) flight during which the 52-GHz channel counts increased out of detectable range (12/03). The large drops in counts are where the aircraft rolled.

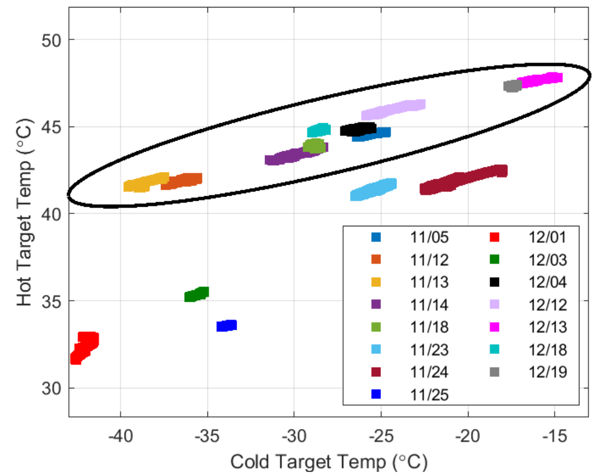

Fig. 6. Hot target versus cold target temperature for all flights after the hot target temperature stabilized (approximately 2 h into the flight). The days circled are used to estimate the hot target temperature for 12/08 and 12/10, where we lost the hot target temperature recording mid-flight.

those flights to be successful since those channels are SSMIS heritage channels and were not essential to the OLYMPEX campaign. Fig. 5 shows the raw radiometer counts for the 11/18 and 12/03 flights, where 11/18 (top) is a nominal operation flight and 12/03 (bottom) is a flight during which the 52-GHz counts increased out of detectable range. On 11/18, after the instrument reached a stable operating temperature, the counts also became stable and remained that way for the rest of the flight. By contrast, the 12/03 flight had several channels that continued to increase in gain throughout the flight, including the 52-GHz channel, which increased rapidly to go out of detectable range.

The final complication during the campaign was the archive computer shutting down mid-flight. The archive computer stores all data during the flight, and the calibration and scan head computers synchronize with the archive computer. Therefore, when the archive computer shuts down, CoSMIR is inoperable. This issue manifested itself when we removed the faulty power supply after the 12/03 flight and ran both the heaters and computer off one power supply for the 12/04–12/10 flights. Everything worked properly for the 12/04 flight; however, the following three flights experienced a failure of the archive computer after a couple of hours. Our attempts to reboot the computer on 12/05 were unsuccessful, and we lost about 3 h of potential data for that flight. On 12/08 and 12/10, we were able to successfully reboot the archive computer, but we lost the computer that records the hot target temperature. The hot target was still being heated properly, but knowing the temperature of the hot target is essential for calibration. We decided to continue recording data and attempt to correct for the missing hot target temperatures in software processing, as will be described in Section III-C.

Once we obtained the new power supply for the heaters, the computer behaved nominally for the last four flights.

C. Quality Control

1) Hot Target Model: In order to produce the calibrated brightness temperatures for the 12/08 and 12/10 flights, we developed a model to estimate the hot target temperature during the time period where it was not recorded. The heaters kept the hot target temperature at a relatively stable temperature during flight; however, it still fluctuated by about 1 K even after it reached a stable value. This is a significant change that impacts the calibration and needs to be accounted for; therefore, it is not accurate to assume a constant hot target temperature. We examined the data from all other flights and found that the hot target temperature for 12/08 and 12/10 can be roughly estimated using the relationship between the hot and cold target temperatures from the other flights. Fig. 6 displays this relationship. Data from the beginning of the flight (approximately 2 h) are excluded to remove the time period before the targets reached a stable operating temperature. The circled data points correspond to flights during which the heater power supply did not undergo a failure. These data points all lie roughly along a line, whereas on the days that the heater power supply failed, the hot target temperature was colder than it should have been. A linear relationship is derived from the data points circled in Fig. 6, and this relationship is used to estimate the hot target temperature based on the recorded cold target temperature for the 12/08 and 12/10 flights. The average cold target temperatures for the 12/08 and 12/10 flights were approximately $-33°$ C and $-21°$ C, respectively, and these values fall within the range of cold target temperatures recorded from the other flights.

To estimate the error in TBs due to this approach, the linear relationship derived from Fig. 6 is used to calculate the hot target temperature from a flight during which we did not experience a computer failure. The difference between the true TB and estimated TB is used to estimate the error in TBs for the 12/08 and 12/10 flights. Fig. 7 shows this

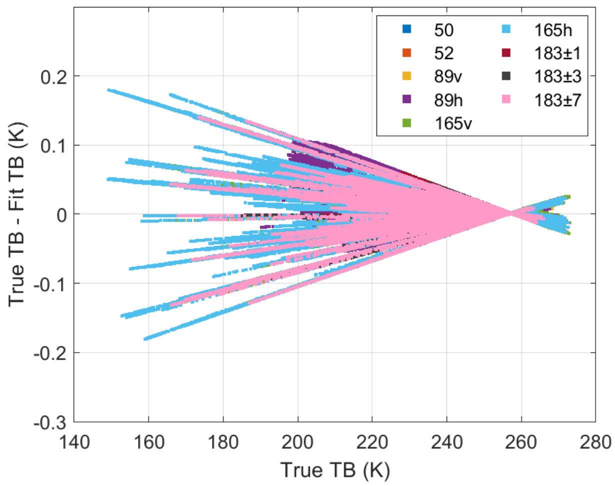

Fig. 7. Error in TB for 12/13 when using the relationship from Fig. 6 to estimate the hot target temperatures. The difference in TB is less than 0.3 K for all channels, so this method can reasonably be used to estimate the hot target temperatures for the 12/08 and 12/10 flights.

error for the 12/13 flight. The error is greatest at the coldest temperatures and equals zero where the TB is equal to the cold target temperature. This flight is chosen for evaluation since it experienced the warmest cold target temperatures, which means that it has the largest error at the coldest temperatures in comparison to the other flights. The difference between the true TB and fit TB is less than 0.3 K, which is an acceptable error, as the accuracy of CoSMIR is approximately 1 K. Most channels have errors less than 0.1 K, and for the 89h and 165h channels that have the greatest number of values larger than 0.1 K, 98% of pixels have a difference less than 0.1 K. The other OLYMPEX flights were evaluated as well and show very similar errors, so we conclude that the error in TB for 12/08 and 12/10 flights is less than 0.3 K.

2) Geolocation: We thoroughly analyzed the CoSMIR footprint geolocation to ensure that the aircraft navigation data were correctly processed and that the azimuth and elevation angles recorded by CoSMIR were accurate. To determine the geolocation accuracy, we superimposed the TBs on Google Earth and looked at coastal crossings in the 89h channel. The CoSMIR 50 and 89v/h channels are sensitive to the surface in most conditions except very high precipitation or thick clouds, and there is a large contrast between the ocean TB and land TB at these frequencies. This contrast is seen in Fig. 4, which shows several coastal crossings. The 89h channel shows the largest difference in TB from land to ocean, so this channel is used here for the geolocation analysis.

One major correction to the recorded CoSMIR azimuth angle was made as a result of analyzing the geolocation. A recorded azimuth angle of 0° assumes that CoSMIR is pointing directly forward in line with the nose of the aircraft. However, after CoSMIR was mounted on the aircraft, we noticed that CoSMIR did not perfectly align with the nose of the aircraft at 0° azimuth. We estimated this azimuth offset by physically rotating the instrument to visually align with the nose of the aircraft and observing the recorded change in azimuth angle on the computer. This offset is estimated to be approximately 4° to the right (clockwise) and was confirmed using Google Earth. Unfortunately, after we replaced the broken azimuth encoder prior to the 11/18 flight, CoSMIR was remounted to the aircraft 18° counterclockwise (to the left) from its original home position. This is a negative azimuth offset, so adding this to the original 4° mounting offset results in a $-14°$ azimuth offset from the nose of the aircraft. This offset was also confirmed using Google Earth and occurs for all flights from 11/18 onward.

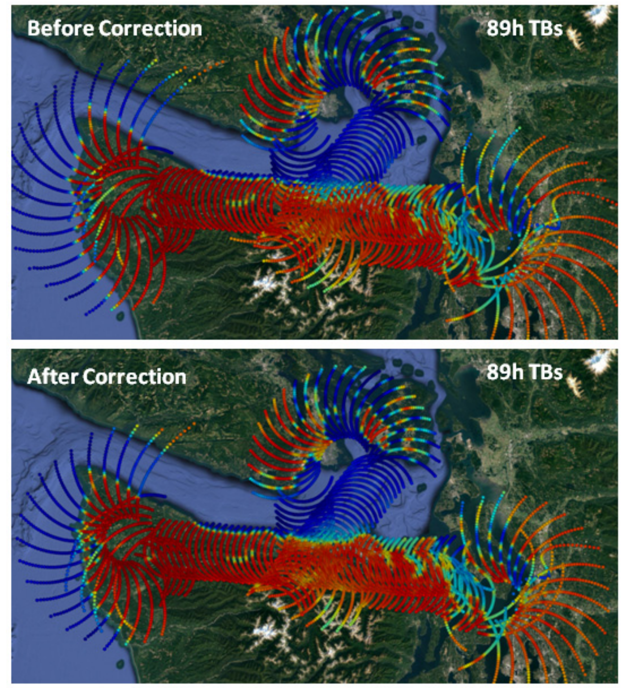

Fig. 8. Google Earth image of 11/24 89h TBs (Top) before and (Bottom) after correcting the azimuth angle. Google Earth was used to confirm the correct geolocation for all flights with observations from coastal crossings.

Fig. 8 shows the Google Earth map of the 89h TBs from the beginning of the 11/24 flight. Fig. 8 (top) shows the uncorrected geolocation, and Fig. 8 (bottom) shows the corrected geolocation (adding a $-14°$ azimuth offset). We analyzed many images like this from several flights, looking at coastlines in several directions. While this method of determining geolocation is prone to human error and lacks precision, we estimate the maximum CoSMIR geolocation error is less than 0.5 km.

IV. Data Analysis

We analyzed the data for accuracy by first comparing the CoSMIR observations with GMI during the flights with a GPM CO overpass and by second looking at the PD of the 89- and 165-GHz channels and comparing it to the literature as well as the GMI measurements.

A. GMI Comparison

The DC-8 coordinated several flights with a GPM CO overpasses to validate GPM's precipitation algorithms and allow comparisons between the similar instruments on the GPM CO and the aircraft. Several of these overpasses were

TABLE III
GMI VERSUS CoSMIR CENTER FREQUENCY, BANDWIDTH, EIA, AND FOOTPRINT COMPARISON

Channel		**Bandwidth (GHz)**		**EIA (nominal)**		**Footprint (km)**	
GMI	*CoSMIR*	*GMI*	*CoSMIR*	*GMI*	*CoSMIR*	*GMI*	*CoSMIR*
89.0 v/h	89.0 v/h	5.9	2.0	52.8	49.3	4.4x7.2	1.3x1.9
166.0 v/h	165.5 v/h	3.8	2.0	49.2	49.3	4.1x6.3	1.3x1.9
183.31±3 v	183.31±3 h	1.6	2.0	49.2	49.3	3.8x5.8	1.3x1.9
183.31±7 v	183.31±7 h	1.9	3.0	49.2	49.3	3.8x5.8	1.3x1.9

also coordinated to align the other two aircraft (ER-2 and Citation) with the DC-8 to obtain coincident measurements among the three aircraft and GPM CO. GMI on GPM CO has been analyzed and shown to be a very well calibrated radiometer [17], so GMI can be used as a calibration reference for determining the accuracy of the CoSMIR observations.

There are a few differences in instrument characteristics between GMI and CoSMIR that need to be taken into account when comparing the two radiometers. The center frequency, polarization bandwidth, earth incidence angle (EIA), and footprint size for GMI and CoSMIR are given in Table III. There is a slight difference in center frequency at the 165-GHz channel, and the polarization is different at the 183-GHz channels. Differences in TB due to the 165 GHz center frequency offset should be minimal, and the PD at 183 GHz will be minimal except in locations of strong convection with oriented cloud ice particles. The bandwidths are also different, especially for the 89-GHz channel, which may cause some small TB differences between GMI and CoSMIR. The large difference in EIA at 89 GHz is a factor that will contribute to fairly large differences in TB over the ocean surface. Due to aircraft pitch and roll changes, the CoSMIR EIA experiences large fluctuations during flight. Therefore, observations with an EIA difference larger than $\pm 3^\circ$ from nominal or aircraft roll larger than $\pm 1^\circ$ are filtered out and not included in the crossover dataset. The nominal EIA for CoSMIR is calculated assuming 0° pitch and roll for the aircraft. In reality, the DC-8 flies with a slight pitch, typically between 1° and 2°. This moves the CoSMIR EIA closer to the GMI EIA for 89 GHz than what is listed in Table III but causes a larger difference between CoSMIR and GMI at the 165- and 183-GHz channels. The last major difference in GMI and CoSMIR is the footprint size. CoSMIR has a smaller footprint size than GMI, and this can cause significant TB differences, where there are heterogeneous areas of precipitation and clouds or surface characteristics. To help mitigate this, the crossover data set includes CoSMIR observations only within 15 min of the GPM CO overpass time and with a distance of less than 1 km between the footprint centers. This gives sufficient data for averaging while keeping similar observations between CoSMIR and GMI of cloud and precipitation structures and the surface.

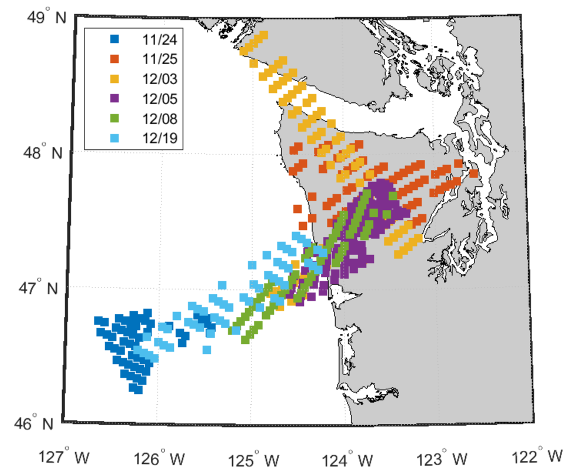

Fig. 9. Locations of CoSMIR/GMI crossover points by date for the 165- and 183-GHz channels. CoSMIR observations within 1 km and 15 min of the GMI pixels are considered a part of the crossover data set.

Fig. 9 shows the location of the crossover points between CoSMIR and GMI by date, and Fig. 10 shows the TB comparison. The GMI 1C V05A data set obtained from the NASA Precipitation Processing System is used for this analysis [18]. There is some significant scatter in the TBs in Fig. 10, mostly attributed to heterogeneous scenes where the difference in footprint sizes between GMI and CoSMIR matters greatly. The difference in EIAs for 89 GHz can be seen most strongly in 89v for the dates that contain several overocean observations, 11/24 and 12/19, where the GMI TBs are significantly warmer than CoSMIR due to GMI's higher EIA. The PD for the 183-GHz channels can also be seen at cold TBs, where the GMI 183-GHz TBs become several Kelvins warmer than the CoSMIR TBs due to areas of strong convection.

A mean TB difference (GMI–CoSMIR) is calculated and shown in Table IV along with the standard deviation. Several filters are applied to arrive at this difference to reduce the scatter seen in Fig. 10. First, all pixels, where 183 ± 3 are warmer than 183 ± 7, are removed, as these indicate the places of potential convection and cloud ice scattering. Areas where the PD (v-pol minus h-pol) at 89- and 165-GHz channels is greater than 10 K are removed, which helps to eliminate the pixels with strong contribution from the polarized ocean

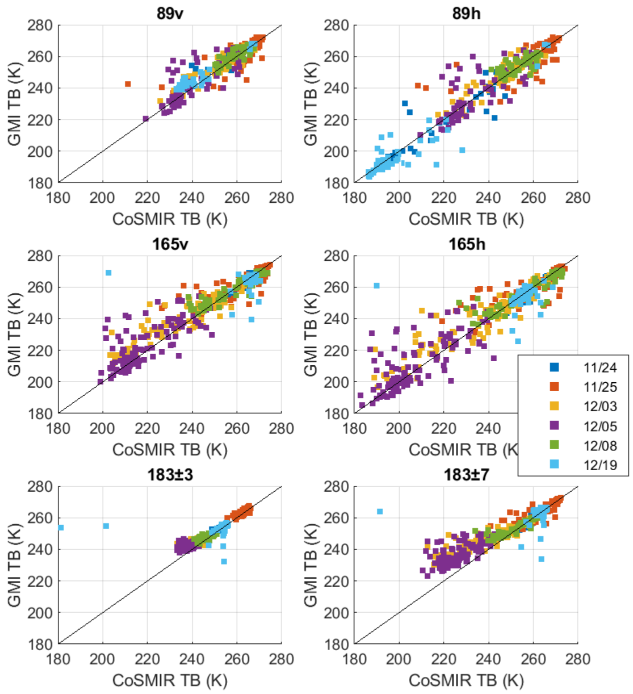

Fig. 10. GMI versus CoSMIR TB for all crossover points. The large scatter in the 89- and 165-GHz channels is mostly due to heterogeneous precipitation regions, and the difference between v-pol (GMI) and h-pol (CoSMIR) for the 183-GHz channels can be seen for convective regions.

TABLE IV
GMI-CoSMIR TB Difference Using the Crossover Points Filtered for Convection and PD at 89 GHz. All Channels Except 165h Have a Mean Difference Within the CoSMIR Accuracy of 1.0 K

	89v	89h	165v	165h	183±3	183±7
Mean (K)	0.37	-0.18	-0.57	-1.09	0.78	0.34
Stnd. Dev. (K)	4.68	5.35	3.22	3.68	1.20	2.08

surface, where the EIA differences have an impact. This also helps to remove the convective regions, where CoSMIR may see larger TB depressions than GMI due to the smaller footprint size. The average CoSMIR EIA for these mean differences is 50.6° with a standard deviation of 0.98° , which indicates that some error due to EIA differences may still contribute to the differences seen in Table IV. There is also the possibility that the CoSMIR EIA has errors due to any uncertainties in how well the instrument pointing is known. The aircraft pitch and roll reported are very accurate, but the elevation and azimuth angles reported by CoSMIR may have errors due to the instrument mounting offsets.

The geolocation analysis showed that the maximum error in geolocation is 0.5 km, which translates to an EIA error of approximately 1°. The error due to GMI observing any atmosphere on top of the DC-8 is determined to be negligible. The contribution of the atmosphere above the aircraft is estimated to be on the order of 0.1 K for the GMI-like channels, as the majority of the water vapor is below the DC-8 altitude of 11.8 km and does not have a significant impact on this comparison. The differences noticed in Table IV are therefore most likely a result of footprint sizes and calibration differences. All channels except 165h have a mean difference within the CoSMIR accuracy of 1.0 K.

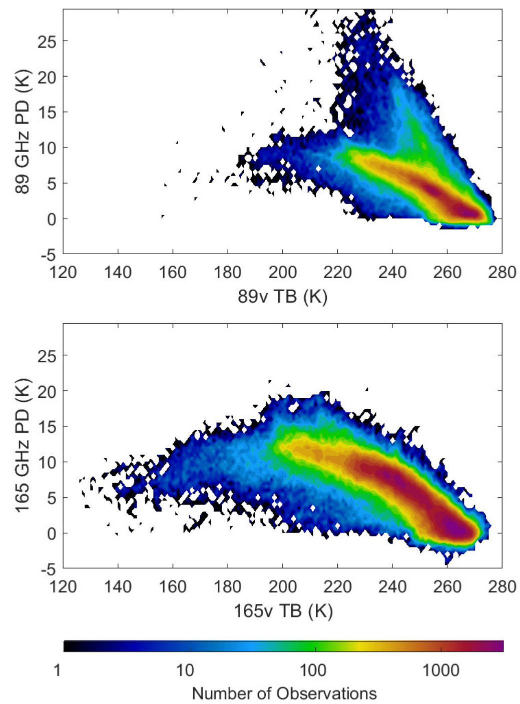

Fig. 11. PD for CoSMIR for all science flights. Colors indicate the number of observations. There is a lack of very cold TBs for 89 GHz, but the shapes are similar to what is expected.

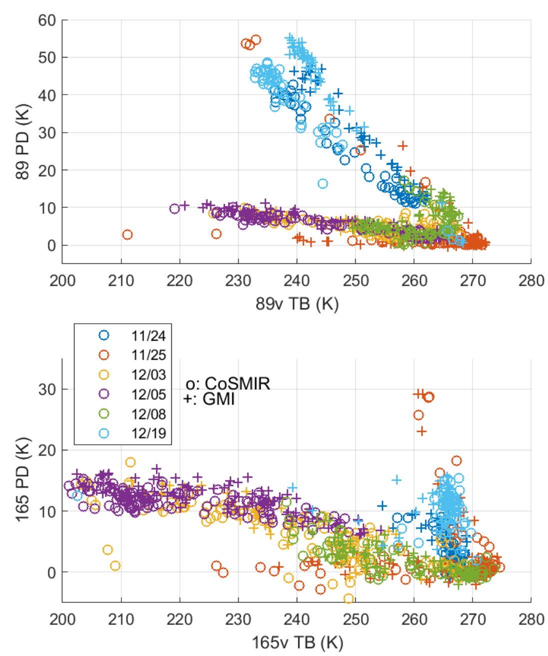

Fig. 12. PDs as a function of v-pol TB for CoSMIR (o symbol) and GMI (+ symbol) crossovers for (Top) 89 and (Bottom) 165 GHz. The PDs for both radiometers show very similar shapes.

B. Polarization Difference

The PD is calculated as the difference between vertically and horizontally polarized TBs. The first spaceborne radiometer with dual polarization near the 165-GHz channel was the Microwave Analysis and Detection of Rain and Atmospheric Structures (MADRAS) instrument onboard Megha-Tropiques, with a center frequency at 157 GHz. Unfortunately, MADRAS encountered performance issues and was eventually turned OFF, but there were still sufficient data to observe the PD signal at 157 GHz from space, although the observations were limited to the tropics [19]. GMI on the GPM CO allows for near-global observations of the PD at 166 GHz and is currently the only spaceborne radiometer with dual polarization at this channel. Gong and Wu [20] looked at the 89- and 166-GHz PD for GMI and found that a maximum PD exists for both frequencies around 200 K–210 K. Panegrossi *et al*. [21] showed the value of the GMI 166-GHz polarization signal in obtaining snowfall retrievals. In this section, we present the CoSMIR PD observations at 89 and 166 GHz to show the accuracy of the CoSMIR measurements in relation to GMI.

Fig. 11 shows 2-D histograms of the CoSMIR PD for 89 GHz (top) and 165 GHz (bottom) as a function of the v-pol TB using all flight data. Colors indicate the number of observations. To help isolate the pixels, where scattering is the main contribution to the top of atmosphere TB, instead of the surface or only absorption, pixels where the 165v(165h) TBs are greater than 89v(89h) are removed. While OLYMPEX did not focus on observing storm structures with strong convection, CoSMIR still recorded some cold TBs at 165 GHz, but this lack of strong convection means that very cold 89v TBs were not observed. However, even with the lack of sufficient cold TB data, it is still apparent that there is a maximum in the curve for both channels around 200 K–210 K, which was seen with GMI [20].

Fig. 12 shows the CoSMIR PD compared with GMI PD, using the crossover data set described previously. The two radiometers give very similar results. The large discrepancy in the 89-GHz PD over the ocean can be seen in the 11/24, 11/25, and 12/19 flights, due to the difference in viewing angles between CoSMIR and GMI.

V. Conclusion

CoSMIR flew on the DC-8 in the OLYMPEX GPM field campaign from November to December, 2015, and obtained a well-calibrated brightness temperature data set of over 72 h of observations. This high-quality data set was a result of extensive updates to the CoSMIR instrument done prior to the campaign as well as improved software processing and analysis. This allowed CoSMIR to collect the highest quality data set in OLYMPEX compared to the prior three GPM campaigns that CoSMIR flew in. The data are publicly available from the GHRC in the HDF5 format [22].

This paper gave a detailed summary of the CoSMIR instrument improvements and the performance during the OLYMPEX campaign. The instrument updates were done to make the instrument more reliable for OLYMPEX and potential future campaigns. CoSMIR was also tested in a thermal chamber, and as a result, we identified an azimuth angle error and striping in the data that we were able to correct prior to deployment. CoSMIR experienced minor performance issues during the campaign, including a broken azimuth encoder, loss of the 50- and/or 52-GHz channels to gain increases, and computer anomalies. The broken azimuth encoder resulted in three flights that only collected data in cross-track scanning mode, which are still useful observations for data users. Losing the 50- and/or 52-GHz channels due to gain increases did not significantly impact our data set, as those channels were not essential to the OLYMPEX campaign. The computer anomalies caused the most significant issues, resulting in the computer shutting down mid-flight a few times and the loss of approximately 4 h of potential data. We were able to mitigate most of these performance issues and were still able to collect a high-quality data set.

Data analysis showed the accuracy of the CoSMIR measurements by comparing with GMI observations during the coordinated GPM CO overpass flights. The GMI-similar channels show a mean difference within 1.0 K between CoSMIR and GMI. The PD at 89 and 165 GHz was also calculated, and the PD results are very similar to what has been seen with GMI observations. These analyses show that the OLYMPEX CoSMIR data set may be reliably used for the algorithm development.

References

[1] A. Y. Hou *et al.*, "The global precipitation measurement mission," *Bull. Amer. Meteorol. Soc.*, vol. 95, pp. 701–722, May 2014.

[2] G. Skofronick-Jackson *et al.*, "The global precipitation measurement (GPM) mission for science and society," *Bull. Amer. Meteor. Soc.*, vol. 98, no. 8, pp. 1679–1695, Aug. 2017.

[3] C. Kummerow and W. A. Petersen. (2006). *GPM Ground Validation: Strategy and Efforts*. [Online]. Available: https://pmm.nasa.gov/sites/default/files/document_files/webdoc2_gv_whitepaper.pdf

[4] D. W. Draper, D. A. Newell, F. J. Wentz, S. Krimchansky, and G. M. Skofronick-Jackson, "The global precipitation measurement (GPM) microwave imager (GMI): Instrument overview and early on-orbit performance," *IEEE J. Sel. Topics Appl. Earth Observ. Remote Sens.*, vol. 8, no. 7, pp. 3452–3462, Jul. 2015.

[5] R. A. Houze, Jr., *et al.*, "The Olympic Mountains experiment (OLYMPEX)," *Bull. Amer. Meteorolog. Soc.*, vol. 90, no. 10, pp. 2167–2188, Oct. 2017.

[6] C. Kummerow, W. Barnes, T. Kozu, J. Shiue, and J. Simpson, "The tropical rainfall measuring mission (TRMM) sensor package," *J. Atmos. Ocean. Technol*, vol. 15, pp. 809–817, Jun. 1998.

[7] C. D. Kummerow *et al.*, "The evolution of the Goddard profiling algorithm to a fully parametric scheme," *J. Atmos. Ocean. Technol.*, vol. 32, no. 12, pp. 2265–2280, Dec. 2015.

[8] R. Bennartz and P. Bauer, "Sensitivity of microwave radiances at 85–183 GHz to precipitating ice particles," *Radio Sci.*, vol. 38, no. 4, pp. 8075–8090, Aug. 2003.

[9] G. Skofronick-Jackson and B. T. Johnson, "Surface and atmospheric contributions to passive microwave brightness temperatures for falling snow events," *J. Geophys. Res.*, vol. 116, pp. D02213-1–D02213-16, Jan. 2011.

[10] Y. You, N.-Y. Wang, R. Ferraro, and S. Rudlosky, "Quantifying the snowfall detection performance of the GPM microwave imager channels over land," *J. Hydrometeorol.*, vol. 18, no. 3, pp. 729–751, Mar. 2017.

[11] I. S. Adams and M. H. Bettenhausen, "The scattering properties of horizontally aligned snow crystals and crystal approximations at millimeter wavelengths," *Radio Sci.*, vol. 47, no. 5, Oct. 2012.

[12] X. Xie, S. Crewell, U. Löhnert, C. Simmer, and J. Miao, "Polarization signatures and brightness temperatures caused by horizontally oriented snow particles at microwave bands: Effects of atmospheric absorption," *J. Geophys. Res. Atmos.*, vol. 120, no. 12, pp. 6145–6160, Jun. 2015.

[13] J. R. Wang, G. M. Skofronick-Jackson, M. R. Schwaller, C. M. Johnson, W. B. Monosmith, and Z. Zhang, "Observations of storm signatures by the recently modified conical scanning millimeter-wave imaging radiometer," *IEEE Trans. Geosci. Remote Sens.*, vol. 51, no. 1, pp. 411–424, Jan. 2013.

[14] G. Skofronick-Jackson *et al.*, "Global precipitation measurement cold season precipitation experiment (GCPEX): For measurement's sake, let it snow," *Bull. Amer. Meteorolog. Soc.*, vol. 96, no. 10, pp. 1719–1741, Oct. 2015.

[15] A. Barros *et al.*, "NASA GPM-ground validation: Integrated precipitation and hydrology experiment 2014 science plan," EPL/Duke Univ., Durham, NC, USA, Tech. Rep. V5, 2014, p. 64. doi: 10.7924/G8CC0XMR.

[16] J. Piepmeier *et al.*, "An airborne conical scanning millimeter-wave imaging radiometer (CoSMIR)," in *Proc. IEEE Geosci. Remote Sens. Symp. (IGARSS)*, vol. 2, Jul. 2001, pp. 894–896.

[17] F. J. Wentz and D. Draper, "On-orbit absolute calibration of the global precipitation measurement microwave imager," *J. Atmos. Ocean. Technol.*, vol. 33, no. 7, pp. 1393–1412, Jul. 2016.

[18] GPM Science Team. (2016). GPM GMI Common Calibrated Brightness Temperatures Collocated L1C 1.5 hours 13 km V05. Goddard Earth Sciences Data and Information Services Center, Greenbelt, MD, USA. Accessed: Dec. 2017. doi: 10.5067/GPM/GMI/GPM/1C/05.

[19] E. Defer, V. S. Galligani, C. Prigent, and C. Jimenez, "First observations of polarized scattering over ice clouds at close-to-millimeter wavelengths (157 GHz) with MADRAS on board the Megha-Tropiques mission," *J. Geophys. Res. Atmos.*, vol. 119, no. 21, pp. 12301–12316, Nov. 2014.

[20] J. Gong and D. L. Wu, "Microphysical properties of frozen particles inferred from global precipitation measurement (GPM) microwave imager (GMI) polarimetric measurements," *Atmos. Chem. Phys.*, vol. 17, pp. 2741–2757, Feb. 2017.

[21] G. Panegrossi, J.-F. Rysman, D. Casella, A. C. Marra, P. Sano, and M. S. Kulie, "CloudSat-based assessment of GPM microwave imager snowfall observation capabilities," *Remote Sens.*, vol. 9, no. 12, p. 1263, 2017.

[22] W. Petersen, R. Houze, and L. McCurdie. (2018). GPM Ground Validation OLYMPEX Field Campaign Data Collection. NASA EOSDIS Global Hydrology Resource Center Distributed Active Archive Center, Huntsville, AL, USA. [Online]. Available: http://ghrc.nsstc.nasa.gov/. doi: 10.5067/GPMGV/OLYMPEX/DATA101.

Rachael A. Kroodsma received the B.S.E. degree in earth systems science and engineering, the M.S.E. degree in electrical engineering, and the Ph.D. degree in atmospheric, oceanic, and space sciences from the University of Michigan, Ann Arbor, MI, USA, in 2009, 2013, and 2014, respectively.

She is currently an Assistant Research Scientist with the Earth System Science Interdisciplinary Center, University of Maryland at College Park, College Park, MD, USA. She is also with the Precipitation Processing System with the NASA Goddard Space Flight Center, Greenbelt, MD, USA. As a member of the Global Precipitation Measurement (GPM) Inter-Calibration Working Group (XCAL), she works on developing intercalibration techniques and monitoring the calibration of the GPM constellation microwave radiometers. She also serves as the Instrument Scientist for the Airborne Conical Scanning Millimeter-wave Imaging Radiometer (CoSMIR). Her research interests include microwave radiometer calibration and remote sensing of the atmosphere from airborne and spaceborne sensors.

Matthew A. Fritts received the B.S. degree in electrical engineering from the University of Maryland, College Park, MD, USA, in 2009. He is currently pursuing the M.S.E. degree in electrical engineering from Johns Hopkins University, Baltimore, MD, USA.

He is currently an Electronics Engineer with the Microwave Instrument and Technology Group, NASA Goddard Space Flight Center, Greenbelt, MD, USA, where he has supported hardware developments on Global Precipitation Measurement (GPM), Soil Moisture Active Passive (SMAP), and CubeSat Radiometer RFI Technology Validation (CubeRRT) spaceflight missions. He also serves as the Instrument Integration and Test Lead for the Signals of Opportunity P-Band Investigation (SNOOPI) cubesat instrument, and as the Lead Engineer of the Conical Scanning Millimeter-wave Imaging Radiometer (CoSMIR) airborne instrument.

Jared F. Lucey received the B.S. degree in electrical engineering from the University of Massachusetts, Amherst, MA, USA, in 2007, and the M.S.E. degree in electrical engineering from Johns Hopkins University, Baltimore, MD, USA, in 2011.

In 2005, he joined the Microwave Instrument and Technology Branch, NASA Goddard Space Flight Center, Greenbelt, MD, USA, where he served as a Lead Engineer on developments for the flight missions Global Precipitation Measurement (GPM) and Soil Moisture Active Passive (SMAP) as well as the CubeSat missions IceCube and CubeSat Radiometer RFI Technology Validation (CubeRRT). He is currently the Associate Branch Head of the Microwave Instrument and Technology Branch and a Lead Engineer on a maturation program for a Submillimeter Enceladus Life Fundamentals Instrument (SELFI).

Mr. Lucey was a recipient of the NASA Agency Award for Exceptional Service in 2017 and the NASA Agency Award for Outstanding Leadership in 2018.

Mathew R. Schwaller, photograph and biography not available at the time of publication.

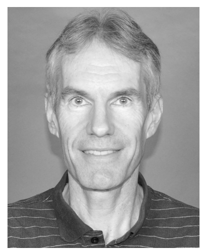

Troy J. Ames received the B.S. degree in mathematics and the B.S. degree in computer science from the University of Idaho, Moscow, ID, USA, in 1984, and the M.S. degree in computer science from Johns Hopkins University, Baltimore, MD, USA, in 1991.

He is currently a Senior Computer Engineer with the Science Data Processing Branch, NASA Goddard Space Flight Center, Greenbelt, MD, USA, where he is leading machine learning projects related to feature detection of remote sensing images and applications to quantum computing.

Mr. Ames was a recipient of the NASA Medal for Exceptional Service in 2000 and the Excellence in Information Science and Technology Award in 2004.

Caitlyn M. Cooke (S'16) received the B.S. and M.S. degrees in electrical engineering from the University of Colorado at Boulder, Boulder, CO, USA, in 2014 and 2016, respectively, where she is currently pursuing the Ph.D. degree in electrical engineering.

From 2014 to 2017, she was with NASA Goddard Space Flight Center, Greenbelt, MD, USA, where she was involved with submillimeter-wave radiometers for CubeSats. She is currently an RF Design Engineer with Northrop Grumman Aerospace Systems, Redondo Beach, CA, USA, where she is focused on high-frequency MMIC design and packaging.

Dr. Cooke received the NASA Space Technology Research Fellowship in 2016, for research on millimeter-wave monolithic microwave integrated circuits for radiometer front ends.

Lawrence M. Hilliard received the B.S. degree in electrical engineering from Michigan Technological University, Houghton, MI, USA, in 1983.

He has been with NASA Goddard Space Flight Center for more than 30 years. He is currently the VLBI Global Observing System (VGOS) Technologist in the Space Geodesy Project (SGP) at Goddard. Prior to SGP, he led an AESMIR aircraft instrument team winning a Robert Goddard Exceptional Achievement Award. He has also managed efforts for cosmic background explorer differential microwave radiometers, submillimeter wave astronomy satellite, and swift burst alert telescope instrument and payload development and has been involved in the formulation and development of numerous aircraft and earth-orbiting spacecraft and payloads. His career started with parts engineering on the GOES program for NASA Goddard.